# Interplay between non-covalent interactions in 1D supramolecular polymers based on 1,4-bis(iodoethynyl)benzene†

Lucia González,[ab] Sara Graus,[b] Blanca Gaspar,[b] Sheila Espasa,[b] Adrián Velázquez-Campoy,[cdef] Julen Munarriz,‡[g] José Luis Serrano, Rosa M. Tejedor[h] and Santiago Uriel*[ab]

A study of the solution-phase, solid-state structures of halogen-bonded co-crystals of 1,4-bis(iodoethynyl)benzene (*p*-BIB) with three salts, namely, decyltrimethylammonium bromide (DTMABr), tetrapropylammonium bromide (TPABr), and tetrabutylammonium bromide (TBABr), has been carried out, along with theoretical calculations. Isothermal titration calorimetry (ITC) showed that the binding constant of bromide with *p*-BIB in THF is not strongly dependent on the cation, and that the entropic term clearly dominates the enthalpic one in the free energy of binding. In the three crystal structures, the bromide anion acts as a doubly connected node for halogen bonding interactions, which results in linear or angular open chains. The intrachain angles (I···$Br^-$···I) of the 1D supramolecular polymers based on *p*-BIB depend on the geometry and size of the cation and vary from 180° for DMTABr to 75° for TBABr. Non-covalent interaction (NCI) analysis of selected motifs and optimized crystals demonstrates that the balance between halogen bonds, hydrogen bonds, and van der Waals interactions, especially type-I halogen···halogen contacts, determines the crystal structures.

## 1. Introduction

When a halogen atom participates in a covalent bond, a very small region on the outer surface of the halogen opposite to the covalent bond exhibits a positive electrostatic potential (σ-hole). In contrast, the belt around the halogen atom is negative due to the densities of the electron lone pairs. Halogen bonding is the attractive interaction between the electrophilic region (σ-hole) and an electron-rich site.[1] The complexation ability of a halogen bond (XB) donor increases with the positive electrostatic potential of the σ-hole, which depends on the polarizability of the halogen (greater in heavier halogens) and the presence of electron-withdrawing moieties. Furthermore, it has been found that higher *s* contribution to the sp hybridization of the *ipso* carbon corresponds to higher halogen bond strength. Thus, attaching an ethynyl group to the halogen atom is a proven strategy to improve the complexation ability of a XB donor.[2]

Bis(haloethynyl)benzene derivatives have proven to be good halogen bond donors due to the deep positive electrostatic potential at the end region of the halogen atoms opposite the C(sp)–X covalent bond (σ-hole).[3,4] Furthermore, the haloethynylbenzene derivatives can establish edge-to-edge intermolecular interactions between the haloethynyl groups and adjacent phenyl rings through C–H···X (X = I, Br) and/or C–H···$\pi_{(alkyne)}$ interactions. These non-conventional hydrogen bonds promote the formation of planar structures.[3] Specifically, the ethynyl groups and iodine atoms of 1,4-bis(iodoethynyl)benzene (*p*-BIB) exhibit a cylindrical negative charge density distribution with which atoms or electropositive groups can interact.[4–6]

Halide anions act as very good XB acceptors due to their negative charge being concentrated on a single atom,[7,8] and their spherical shape allows for the formation of up to eight

[a] *Instituto de Nanociencia y Materiales de Aragón (INMA), CSIC-Universidad de Zaragoza, Zaragoza, Spain. E-mail: suriel@unizar.es*
[b] *Departamento de Química Orgánica, Universidad de Zaragoza, Zaragoza, Spain*
[c] *Department of Biochemistry and Molecular & Cellular Biology, Institute for Biocomputation and Physics of Complex Systems (BIFI), Joint Units IQFR-CSIC-BIFI and GBsC-CSIC-BIFI, Universidad de Zaragoza, Zaragoza, Spain*
[d] *Aragon Institute for Health Research, Zaragoza, Spain*
[e] *Biomedical Research Network Center in Hepatic and Digestive Diseases (CIBERehd), Madrid, Spain*
[f] *ARAID Foundation, Gobierno de Aragón, Zaragoza, Spain*
[g] *Departamento de Química Física, Instituto de Biocomputación de Sistemas Complejos (BIFI), Universidad de Zaragoza, Zaragoza, Spain*
[h] *Centro Universitario de la Defensa, Academia General Militar, Zaragoza, Spain*

halogen bonds.[9] However, it has been observed that halides have a moderate bias towards the formation of two or three halogen bonds. For instance, the co-crystallization of 1,4-diiodotetrafluorobenzene (bidentate XB donor) with halide salts yields linear, angular (with C–Hal···$X^-$···Hal–C angles from 180° to just over 60°) or helical polymeric structures.[10,11] It has recently been reported that the crystallization of 2,6-bis(iodoethynyl)pyridine with different halide salts produces a variety of structural motifs, such as polymeric propellers or discrete macrocycles (with C–Hal···$X^-$···Hal–C angles in the range 77–95°).[11] The presence of acute angles in halide coordination by halogen bonds is not uncommon, even when the halide coordination sphere is formed by only two halogen bonds.[10–15] In general, a decrease in the angle is associated with a longer length and a lower interaction energy of the halogen contact. Fourmigué *et al.* suggested that these geometric arrangements are produced by the existence of significant dispersion forces between the halogen atoms.[10]

The NCI methodology[16] allows the identification and visualization of weak interactions such as hydrogen[3] and halogen bonds.[17] Moreover, it has also allowed the demonstration of contacts that do not exhibit a reduction of the interatomic distance calculated as the sum of tabulated ionic, van der Waals or ionic van der Waals radii.[18]

Taking the above considerations into account, we report here a combined experimental and computational study of the linkage of 1,4-bis(iodoethynyl)benzene (*p*-BIB) with three bromide salts (1 : 1 stoichiometry) having cations with different sizes and geometries, from linear decyltrimethylammonium bromide (DTMABr) to globular tetrapropylammonium bromide (TPABr) and tetrabutylammonium bromide (TBABr). Given the confirmed edge-to-edge contacts of iodoethynylbenzene derivatives and the flexibility of halide coordination spheres with respect to halogen bonds, the size and geometry of the cation of the halide salt co-crystallized with 1,4-bis(iodoethynyl)benzene can tune new supramolecular architectures. The NCI index has been applied to characterize the non-covalent interactions of the synthetized co-crystals and to establish how the size and geometry of the cation influence the weak interactions that support the crystal structures.

# 2. Experimental

### 2.1. Materials

1,4-Bis(ethynyl)benzene, *N*-iodosuccinimide and silver nitrate were purchased from Aldrich. All reagents and solvents were commercially available and were used without further purification. Solution $^1$H and $^{13}$C NMR spectra were recorded at ambient temperature using a Bruker Avance 400 spectrometer (9.4 T, 400.13 MHz for $^1$H, 100.62 MHz for $^{13}$C). Melting points were measured using a Stuart melting point apparatus.

### 2.2. Synthesis of 1,4-bis(iodoethynyl)benzene (p-BIB)

*N*-Iodosuccinimide (4.14 g, 36.2 mmol) and silver nitrate (0.62 g, 3.62 mmol) were added successively to a solution of 1,4-diethynylbenzene (2.28 g 18.1 mmol). The reaction mixture was stirred at 0 °C for 5 h. The reaction mixture was filtered, the funnel was washed with diethyl ether and the solvent was removed under reduced pressure. The residue was dissolved in $CH_2Cl_2$ (50 mL) and extracted with water (3 × 50 mL). The organic layer was dried over $MgSO_4$ and evaporated. The pure product was recovered as a yellow solid (5.13 g). Yield: 75%. MP: 129 °C. $^1$H NMR (400 MHz, $CDCl_3$) $\delta$ = 7.36 (s, 4H); $^{13}$C NMR (75 MHz, $CDCl_3$) $\delta$ = 9.1, 93.7, 123.9, 132.3.

### 2.3. Isothermal titration calorimetry

Calorimetric titrations were performed using a high-sensitivity VP-ITC microcalorimeter (MicroCal, Malvern-panalytical). Solutions of bromide anions as tetraalkylammonium salts (5 mM) in dry degassed THF were titrated into *p*-BIB solutions (0.5 mM) also in THF at 298 K in a 1.4354 mL calorimetric cell. The experimental protocol consisted of 28 10 μL injections, with a 250 s interval between injections, a stirring speed of 459 rpm, and high-feedback gain. The thermograms (thermal power as a function of time, Fig. S1 in the ESI†) were converted to interaction isotherms (ligand-normalized heat effect per injection as a function of molar ratio). The interaction isotherms were analyzed by applying non-linear least-squares regression data analysis (Levenberg–Marquardt algorithm) assuming a 1 : 1 stoichiometry for the *p*-BIB : bromide anion interaction using fitting routines implemented in Origin 7.0 (OriginLab). For each interaction, the association constant, interaction enthalpy, and stoichiometry were estimated as adjustable parameters.

### 2.4. Crystal synthesis

Co-crystals of the ditopic halogen bond donor *p*-BIB and three bromide salts, {p-BIB·DTMDABr} (**1**), {*p*-BIB·TPABr} (**2**), and {*p*-BIB·TBABr} (**3**), were prepared by the slow evaporation of $CH_2Cl_2$ solutions of equimolecular quantities of *p*-BIB and the corresponding bromide salt.

### 2.5. Single crystal X-ray diffraction analysis

The crystals were air stable, and X-ray diffraction experiments were carried out using an Oxford-diffraction Xcalibur S diffractometer. Data were collected at 150(2) K using Mo-Kα radiation. The software packages XSCANS[19] and CrysAlis[20] were used to process data. Final cell parameters were obtained by global refinement of the reflections obtained from the integration of all the frame data. The structures were solved by direct methods and refined by the full-matrix method based on $F^2$ using the SHELXTL program.[21] Non-hydrogen atoms were refined anisotropically and hydrogen atoms were observed in difference electron density maps and refined isotropically. The crystal parameters and basic information related to data collection and structure refinement for co-crystals **1–3** are summarized in Table S1. CCDC 1979343–1979346 ESI.†

### 2.6. Hirshfeld surface analysis

Hirshfeld surfaces and the associated fingerprint plots were calculated using CrystalExplorer,[22] which accepts a structure input file in CIF format. Bond lengths to hydrogen atoms were

set to typical neutron values (C–H = 1.083 Å, N–H = 1.009 Å, O–H = 0.983 Å).[23,24] The distance from the Hirshfeld surface to the nearest atoms outside and inside the surface are characterized by the quantities $d_e$ and $d_i$, respectively, and the normalized contact distance calculated as $d_{norm} = ((d_i - r_i^{vdW})/r_i^{vdW} + (d_e - r_e^{vdW})/r_e^{vdW})$, where $r_i^{vdW}$ and $r_e^{vdW}$ are the vdW radii of the atoms. Plotting $d_e$ *versus* $d_i$ as a 2-D histogram produces a fingerprint plot for each co-crystal.

### 2.7. Computational methods

Electronic structure quantum mechanical calculations in the gas phase were performed using the Gaussian 09 package.[25] Single point calculations of the dimers extracted from experimental crystal structures (Fig. S2 in the ESI†) were carried out using DFT with the B3LYP exchange–correlation functional[26–28] and Grimme D3BJ dispersion correction scheme.[29,30] The 6-311G+(d,p) or 6-311G++(d,p) basis set[31] was used for all atoms except the halogen atoms, for which the DGDZVP basis set was employed, all in conjunction with a fine integration grid.[32] The trimers extracted from experimental crystal structures (Fig. S2, ESI†) were optimized using the same method and the 6-311G+(d,p)/DGDZVP basis set. The optimizations were performed by means of the Berny Optimization Algorithm as implemented in the Gaussian09 package.[33] While the optimization of (IBrI)-180 was conducted without geometry restrictions, the I···Br···I angles of (IBrI)-75 and (IBrI)-139 were constrained to their experimental values, *i.e.*, 75° and 139°, respectively. We compared the validity of the aforementioned basis set combinations using Ahlrich's triple-zeta def2TZVP basis set for all atoms[34] with an ECP-28 electron core potential for the iodine atoms.[35] Similar results and the same tendencies were obtained (as shown in Table S2, ESI†). Analytical frequencies were calculated and employed to characterize the stationary points as minima by checking that they did not present any imaginary frequencies. The interaction energies between the different monomers that formed part of the complexes (extracted dimers or optimized trimers) were calculated at the same level of theory as the difference between the total complex energy and the sum of the total energies of the monomers. The interaction energies ($\Delta E$) were corrected ($\Delta E_{BSSE}$) using the Boys–Bernardi counterpoise method in order to correct the basis set superposition error (BSSE).[36] Moreover, the interaction energies of the optimized complexes were corrected for scaled (0.9887)[37] zero-point energy differences (obtained from the frequency calculations described above).

The DFT calculations of the crystal structures were performed using the Vienna Ab initio simulation package (VASP), version 5.4.1.[32–34] Optimizations of the three crystals were carried out using the revPBE functional[35] in conjunction with the Grimme D3BJ empirical dispersion scheme.[27] GGA functionals have been reported to yield inaccurate results in some halogen-based systems.[38] To test its performance, we benchmarked the aforementioned scheme with the meta-GGA SCAN functional[38] with and without dispersion corrections (D3 and D3BJ schemes). We chose this functional based on its outstanding performance in the description of both energies and structures in a variety of periodic systems.[38] As shown in Tables S3 and S4 (ESI†), the revPBE-D3BJ results are quite similar to the SCAN and experimental results, but require lower computational effort; hence, we selected the revPBE-D3BJ scheme to carry out the studies. We note that we could not include crystal **3**, {*p*-BIB·TBABr}, in the benchmarking because its unit cell was significantly larger than those of **1** and **2** (280 atoms *vs.* 122 and 116, respectively), which made optimization with the SCAN functional computationally unaffordable for us. The projector augmented wave (PAW)[38,39] method was used to represent the interactions between the core and valence electrons; namely, we included 7 valence electrons for iodine and bromine, 5 for nitrogen, 4 for carbon and 1 for hydrogen atoms. A plane wave cutoff of 400 eV was used for all elements. 5 × 3 × 4, 4 × 5 × 4 and 3 × 5 × 3 Monkhorst–Pack *k*-point meshes were used for {*p*-BIB·DTMABr}, {*p*-BIB·TPABr} and {*p*-BIB·TBABr}, respectively.

Non-covalent interactions were analyzed by means of the NCI index.[39] This approach is based on the analysis of the reduced density gradient of the electron density, $s(\rho)$, and allows the identification and visualization of weak interactions. Specifically, these interactions are unraveled by plotting $s(\rho)$ as a function of the sign of the second eigenvalue of the electron density Hessian ($\lambda_2$) multiplied by the electron density, $\mathrm{sign}(\lambda_2)\rho$. Non-covalent interactions give rise to peaks with low $s(\rho)$ values in the low-electron density zone. The $\mathrm{sign}(\lambda_2)\rho$ value range in which these peaks are found allows the interaction to be characterized. Specifically, vdW interactions have values of $\mathrm{sign}(\lambda_2)\rho \approx 0$; stronger attractive interactions, such as hydrogen bonds, exhibit $\mathrm{sign}(\lambda_2)\rho$ values of $<0$; and steric clashes appear in the $\mathrm{sign}(\lambda_2)\rho > 0$ zone. These interactions can be visualized by plotting the isosurfaces of $s(\rho)$ and coloring them according to the value of $\mathrm{sign}(\lambda_2)\rho$. Specifically, strong attractive interactions are depicted in blue, weak interactions in green and strong repulsive interactions in red. Moreover, the shape of the isosurface provides information regarding the spatial localization of the interactions: dispersive interactions appear as extended and diffuse surfaces, while localized interactions (such as hydrogen and halogen bonds) are characterized by well-defined disk-shaped isosurfaces. NCI analyses of the molecular and crystal structures were performed using NCIPLOT[40] and critic2,[41] respectively. Tridimensional NCI plots were represented using VESTA.[42]

## 3. Results and discussion

Several mild and convenient methods for the preparation of haloalkynes have recently been developed, most of which involve terminal alkynes.[43,44] From among these methods, we selected the one based on the electrophilic iodination of terminal alkynes with *N*-iodosuccinimide and an Ag(I) catalyst due to its experimental ease, mild reaction conditions and high efficiency.[45,46]

### 3.1. Isothermal titration calorimetry

Isothermal titration calorimetry (ITC) is the most accurate, sensitive and rapid technique for obtaining thermodynamic

Table 1 ITC data for *p*-BIB with bromide salts (DMTABr, TPABr, and TBABr) in THF[a]

| Cation | $K_a$ | $\Delta G$ (kJ mol$^{-1}$) | $\Delta H$ (kJ mol$^{-1}$) | $-T\Delta S$ (kJ mol$^{-1}$) | $N$ |
|---|---|---|---|---|---|
| DTMA | $8.3 \times 10^3$ | −22.4 | −0.4 | −22.0 | 1.1 |
| TPA | $2.8 \times 10^3$ | −19.7 | −0.4 | −19.3 | 1.1 |
| TBA | $7.9 \times 10^3$ | −22.2 | −0.8 | −21.4 | 1.2 |

[a] Relative error for $K_a$ is 30%, absolute error for $\Delta H$ and $-T\Delta S$ is 1.3 kJ mol$^{-1}$, absolute error for $\Delta G$ is 0.4 kJ mol$^{-1}$, and absolute error for $N$ is 0.1.

data for molecular interactions in solution. In fact, ITC is the only method that allows the experimental determination of enthalpies in solution.[47,48] This calorimetric technique has rarely been used for the characterization of halogen bonding. The few published studies mainly deal with cationic halogen bond donors such as 2-iodoimidazolium[49,50] or iodo-1,2,3-triazolium derivatives;[51] to date, bis(iodoethynyl)benzene complexes have not been studied.

Supramolecular interactions in solution involve the formation and breakage of weak bonds. These reversible phenomena involve not only the molecular species under investigation, but also the rearrangement of the solvation layer of all participating partners. The heat produced or consumed due to the formation and breakage of an interaction is the result of multiple simultaneous events in a global response. Calorimetry provides experimental data associated with these phenomena, although the connection between molecular behavior and structural detail is frequently open to interpretation.

In this study, isothermal calorimetric titrations (ITC) were carried out in THF to investigate the halogen bond strength of the bidentate *p*-BIB XB donor towards the bromide anion in solution (Fig. S1 in the ESI†). The binding constants (which are translated into free energies $\Delta G$) and the stoichiometric coefficient ($N$) are provided in Table 1, along with the $\Delta H$ and $\Delta S$ values. The binding affinities (Table 1) showed little dependence on the weakly coordinating counteranions of the bromide salts, although they increased slightly with the solubility of the salt.

The determined binding constants are one order of magnitude lower than those reported for 2′,3,3′,3″,4,4″,5,5′,5″,6′-decafluoro-2,2″,6,6″-tetraiodo-1,1′:4′,1″-terphenyl and bromide in THF ($K_a = 6.6 \times 10^4$). In this case, the entropic part of the binding plays a minor role in determining the free energy ($\Delta G^\circ$).[52] In contrast, in the association of iodoimidazolium derivatives (cationic XB donors) with halides, the entropic term represents more than 50% of the overall free energy of binding.[49,50] Surprisingly, the enthalpic contribution ($\Delta H^\circ$) to the overall binding free energy plays a minor role for the neutral halogen bond donor (*p*-BIB) used in this study. The inclusion of an entropy term is crucial, since the data based solely on the $\Delta H^\circ$ values do not take into account a substantial proportion of the global interaction energy.

### 3.2. Crystal structures

Co-crystals of the ditopic halogen bond donor *p*-BIB and three bromide salts, {*p*-BIB·DTMABr} (**1**), {*p*-BIB·TPABr} (**2**) and {*p*-BIB·TBABr} (**3**), were prepared by slow evaporation of dichloromethane solutions of equimolecular quantities of *p*-BIB and the corresponding bromide salt at room temperature. The crystal parameters and basic information regarding data collection and structure refinement for **1** to **3** are summarized in Table S1 (ESI†).

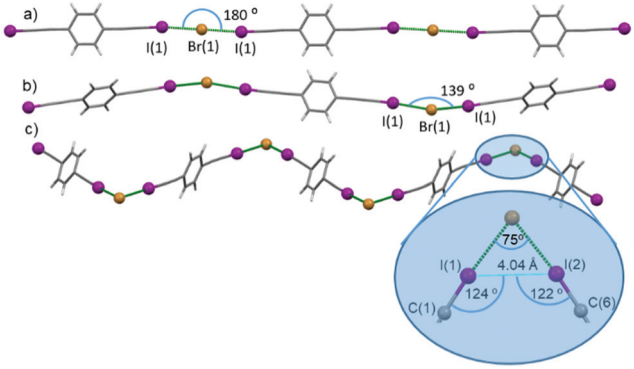


Fig. 1 Details of the non-covalent open chains in: (a) {p-BIB·DTMABr} (**1**); (b) {p-BIB·TPABr} (**2**); and (c) {p-BIB·TBABr} (**3**). The dashed green lines denote halogen bonds.

The crystal structures of the heteromeric three-component systems **1** to **3** exhibit open chains joined by halogen bonds, where the *p*-BIB and the bromide anion alternate and behave as doubly connected nodes. As shown in Fig. 1, the infinite chains adopt linear or zig-zag arrangements. The I···Br$^-$···I angle ranges from 180° in structure **1** to an acute angle of 75° in the structure of **3**, while the structure of **2** has an intermediate angle (139°).

The relevant halogen bond distances (I···Br$^-$) are provided in Table 2, along with the C–I···Br$^-$ and I···Br$^-$···I angles for the compounds studied. The I···Br$^-$ halogen bond distances range from 3.16 to 3.27 Å. These distances correspond to a shortening of the sum of the iodine van der Waals (vdW) radius (1.98 Å) and bromine Pauling ionic radius (1.95 Å) by a factor of 0.80 to 0.83. The C–I···Br$^-$ interactions are approximately linear, with angles ranging from 174.0 to 176.3°.

Examination of the intrachain bond distances and angles shows that decreasing I···Br$^-$···I angle is associated with elongation of the $C_{sp}$–I···Br$^-$ length, which indicates weakening of the halogen bond. It is worth highlighting that the acute angle (75°) present in the halogen-bonded chains in **3** leads to a distance of 4.04 Å between the iodine atoms (Fig. 1c). Despite the fact that it is not less than the sum of vdW radii, this distance, coupled with the C–I···I angles of 122 and 124°

Table 2 Geometric characteristics of the halogen bond interactions; $R_i$ = (I···Br$^-$)/(rvdW1 + rvdW2), where rvdW1 is the vdW radius of iodine (1.98 Å) and rvdW2 is the Pauling ionic radius of bromine (1.95 Å)

| Comp | C–I (Å) | I···Br$^-$ (Å) | C–I···Br$^-$ (°) | I···Br$^-$···I (°) | $R_i$ |
|---|---|---|---|---|---|
| p-BIB | 1.980 | | | | |
| **1** | 2.012 | 3.1594 | 174.4 | 180.0 | 0.80 |
| **2** | 2.024 | 3.2091 | 176.3 | 139.0 | 0.82 |
| **3** | 2.024 | 3.274 | 174.0 | 75.3 | 0.83 |

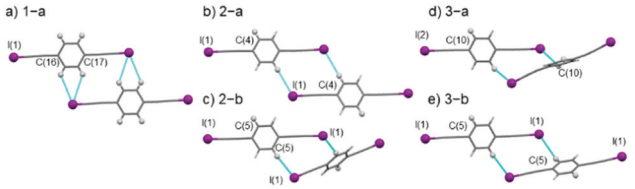


Fig. 2 Depictions of *p*-BIB edge-to-edge interactions in the X-ray crystal structures of (a) {*p*-BIB·DTMABr} (**1**), (b) and (c) {*p*-BIB·TPABr} (**2**), and (d) and (e) {*p*-BIB·TBABr} (**3**). The dashed blue lines denote hydrogen bonds.

observed in **3** (Fig. 1c), suggests a type I halogen–halogen contact, which is usually considered to be dispersive.[53]

The chains linked by halogen bonds show edge-to-edge interactions through non-conventional hydrogen bonds that are formed between the iodine atom and one or two aromatic hydrogens of the adjacent *p*-BIB molecules. Five types of these interactions are found in the structures of **1** to **3**, with two of them being coplanar and three angular (Fig. 2). The edge-to-edge hydrogen bond distances and angles are provided in Table 3.

Coplanar interactions are evident in the structures of **1** (1-a, Fig. 2a) and **2** (2-a, Fig. 2b). They differ in that a bifurcated non-conventional hydrogen bond is formed between the hydrogens linked to C(16) and C(17) and the iodine I(1) atom in the former case. The angles of these hydrogen bonds in **1** deviate more from linearity than those that give rise to the coplanar edge-to-edge interaction in **2**. This latter synthon is similar to that found in the {tris(bis(ethylenedithio)tetrathiafulvalene)·*p*-BIB·Br} cation radical salts described by Yamamoto.[54]

The angular edge-to-edge synthons found in the structures of **2** (Fig. 2c) and **3** (Fig. 2d and e) differ in the angle formed by the planes containing the *p*-BIB molecules. These planes form an angle of 105° in **2** (2-b) and 73° in **3**.

The combination of halogen bonding and edge-to-edge interactions gives rise to flat planes in **1**, corrugated planes in **2** and to a three-dimensional lattice in **3**. The flat sheets in **1** are practically perpendicular to the *b* axis and are separated by 7.3 Å. The DTMA cations in **1** are located between the planes and complete the bromide anion coordination sphere through hydrogen bonds with hydrogen atoms on the α-carbon atom relative to the nitrogen atom. This organization can be facilitated by the elongated geometry and similar lengths of the DTMA cation (15.48 Å) and the [*p*-BIB·Br]$^-$ assembly (15.22 Å). The corrugated planes in **2** along the *ac* plane are separated by 6.9 Å, and the TPA cations are intercalated in this interplanar space. Each of these cations forms two hydrogen bonds with iodine atoms ($Csp^3$–H···I 3.086 Å, 160.4°) (Fig. 3). Fig. S3 (ESI†) shows projection views of **1** and **3**, which demonstrate the layered nature of the anionic and cationic networks.

Table 3 Hydrogen bond distances and angles in the crystal structures of **1–3**

| Comp | D–H···A | *d*(H···A) Å | *d*(D···A) Å | ∠(DHA)° |
|---|---|---|---|---|
| **1** | C(16)–H···I(1) | 3.28 | 3.953 | 131 |
| | C(17)–H···I(1) | 3.33 | 3.977 | 129 |
| **2** | C(4)–H···I(1) | 3.1776 | 4.103 | 173.6 |
| | C(5)–H···I(1) | 3.2171 | 4.063 | 152.1 |
| **3** | C(5)–H···I(1) | 3.1983 | 3.945 | 138.6 |
| | C(10)–H···I(2) | 3.3543 | 3.973 | 126 |

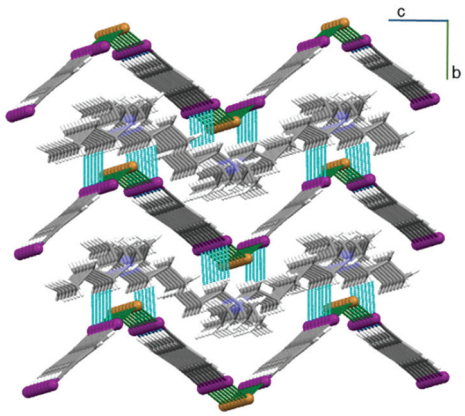


Fig. 3 A projection view of **2** showing the layered nature of the anionic and cationic networks. The dashed green lines denote halogen bonds and the dashed blue lines denote hydrogen bonds.

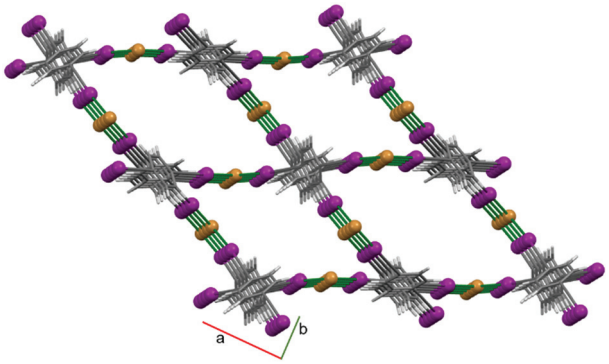


Fig. 4 A projection view of the [(p-BIB)·Br]$^-$ anionic network of **3**, which shows the cavities along the *c* axis.

In the structure of **3** (Fig. 4) the I···Br$^-$···I angle is 75.3° and the chains form angles of 52.01° with each other, which gives rise to an anionic three-dimensional lattice with interconnected cavities. They represent 68% (1998.1 Å$^3$) of the free volume of the unit cell (2940.1 Å$^3$) and this space is occupied by the TBA cations.

### 3.3. Hirshfeld surface analysis

Hirshfeld surfaces provide a three-dimensional image of the close contacts in a crystal. The mapping of the normalized contact distance ($d_{norm}$) on the Hirshfeld surface (red for $d_{norm} < 0$, contacts closer than the sum of the vdW radii and blue for $d_{norm} > 0$, longer contacts) allows identification of the molecular regions involved in short contacts. This information can be summarized by plotting the internal distance ($d_i$: distance from the surface to the nearest atom in the molecule itself) *versus* the external distance to the surface ($d_e$).[55,56]

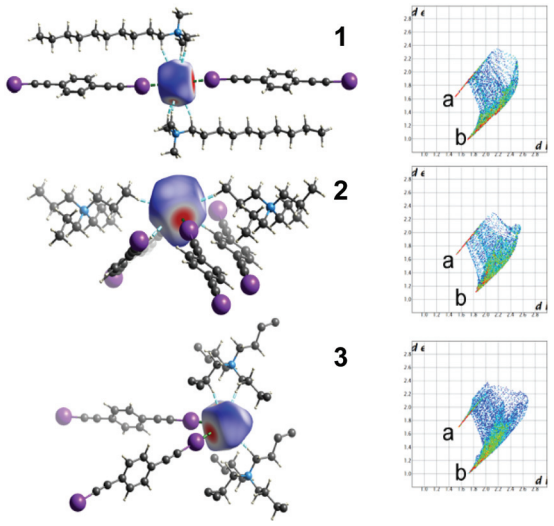


Fig. 5 Anion coordination spheres and Hirshfeld surfaces of the bromide anions in the structures of **1** to **3**, mapped using $d_{norm}$ (left) and fingerprint plots (right).

The Hirshfeld surfaces of *p*-BIB are characterized by a large red spot at the polar end of each of the iodine atoms, which corresponds to the C–I···Br$^-$ halogen bond. In the fingerprint plot, this interaction appears as a line that runs from approximately $d_i$ = 1.7 Å, $d_e$ = 1.5 Å to $d_i$ = 2.0 Å, $d_e$ = 1.9 Å (Fig. S4a in the ESI†). The iodine atoms also establish hydrogen bonds and a type I iodine–iodine contact.[53] These latter contacts appear in the fingerprint graphs of structures **1** and **3** as lines centered on $d_i$ = 2.3 Å, $d_e$ = 2.3 Å and $d_i$ = 2.1 Å, $d_e$ = 2.1 Å, respectively (Fig. S4b in the ESI†).

In all cases, the bromide anion acts as an acceptor for two halogen bonds, as pointed out above. These interactions appear as two large red spots on the Hirshfeld surface of bromide and as a spike in the fingerprint plots labeled as 'a' in Fig. 5. In the fingerprint plots of the three structures, it is clear that peak 'a' shifts to higher values of $d_i$ and $d_e$ from structure **1** to **3**. This change indicates an increase in the halogen bond distance in the same order.

As shown in Fig. 5, the bromide anion in **1** forms six hydrogen bonds with two DTMA cations. The most electrophilic hydrogen atoms form the six interactions, since they are located on the carbon atoms adjacent to the positively charged nitrogen atom. This gives rise to strong hydrogen bonds, as evidenced by the intensity of the red color and the spike labeled 'b'. The situation is very different in **2**, since the bromide anion forms hydrogen bonds with two molecules of *p*-BIB and with some of the less-electrophilic hydrogens of two TPA cations. For this reason, peak 'b' is less pointed than that in structure **1**. Finally, in **3** the situation is intermediate, since the hydrogen bonds are formed with hydrogens of different electrophilic character in two TBA cations.

### 3.4. Theoretical calculations

The electron density map of optimized *p*-BIB (Fig. 6) shows the characteristic positive electrostatic potential at the terminal

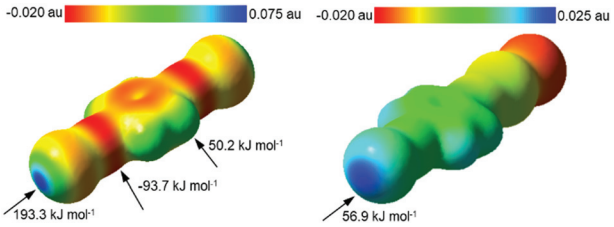


Fig. 6 Computed electrostatic potentials of the optimized geometries of *p*-BIB (left) and the complex [*p*-BIB·Br]$^-$ (right). Potentials are mapped on the respective electron density isosurfaces (0.002 e bohr$^{-3}$).

region of the iodine atoms along the C–I bond. This corresponds to the σ-holes, which are surrounded by an electronegative belt around the axis defined by the C–I bond. Moreover, the electrostatic potential surface indicates that the negative charge is mainly located around the C–C triple bonds. As expected, a positive electrostatic potential is found on the aromatic hydrogen atoms. According to the electrostatic potential surface, *p*-BIB can act as a halogen bond donor and acceptor as well as a non-conventional hydrogen bond acceptor and donor.[3,4] As expected, when one of the iodine atoms is engaged in a halogen bond with the bromide anion (dimer [*p*-BIB·Br]$^-$), the maximum value of the surface electrostatic potential at the non-bonded iodine atom decreases by up to 56.9 kJ mol$^{-1}$, but its halogen-bond-donor ability (σ-hole) is retained. The computed electrostatic potentials of the optimized trimers (IBrI)-75, (IBrI)-139 and (IBrI)-180 are shown in Fig. S5 in the ESI.† As expected, the $V_{max}$ of the trimers is higher than that of the dimer [*p*-BIB·Br]$^-$.

The halogen bond trimers extracted from the structures of **1**, **2** and **3**, which are denoted as (IBrI)-180 (I···Br$^-$···I angle, 180°), (IBrI)-139 (I···Br$^-$···I angle, 139°) and (IBrI)-75 (I···Br$^-$···I angle, 75°) (Fig. S2 in the ESI†), respectively, were optimized using DFT (see Experimental section). The interaction energies and selected geometrical parameters of the optimized halogen bond trimers and the dimer [*p*-BIB·Br]$^-$ are gathered in Table 4.

The calculated interaction energies are within the range of those reported for contacts between similar halogen bond donors and the bromide anion.[14] The geometries of the optimized trimers are consistent with the experimental observations. All of the structures have two identical I···Br$^-$ distances that are smaller than the sum of the vdW radius (1.98 Å) and Pauling ionic radius of bromine (1.95 Å), and the C–I···Br$^-$ angle is linear. As expected, the calculated I···Br$^-$ distances are longer than those corresponding to the optimized dimer [*p*-BIB·Br]$^-$. According to the experimental results, (IBrI)-75 has the longest halogen bond distance (3.229 Å), which indicates a relatively weak halogen bond. However, the calculated interaction energy of (IBrI)-75 is not consistent with the generally accepted trend that a longer contact distance corresponds to a lower interaction energy. Table S5 (ESI†) collects the interaction energies and distances of the I···Br$^-$ contact of optimized [*p*-BIB·Br]$^-$ and similar dimers extracted from the corresponding optimized trimer (B3LYP-D3 and 6 311G+(d,p)/DGDZVP). These data prove that a shorter contact distance is associated with a lower interaction energy.

Table 4 Uncorrected and corrected interaction energies[a] ($\Delta E$ and $\Delta E_{BSSE}$, respectively) and the geometric parameters of [p-BIB·Br]$^-$ and the trimers optimized using B3LYP-D3 and 6-311G+(d,p)/DGDZVP

| Complex | $\Delta E$ (kJ mol$^{-1}$) | $\Delta E_{BSSE}$ (kJ mol$^{-1}$) | $d$(C–I) (Å) | $d$(I···Br$^-$) (Å) | ∠(C–I···Br$^-$) | $R_i$[b] |
|---|---|---|---|---|---|---|
| [p-BIB·Br]$^-$ | −103.3 | −98.7 | 2.113 | 3.030 | 180.0 | 0.77 |
| (IBrI)-180 | −162.3 | −153.1 | 2.065 | 3.168 | 180.0 | 0.81 |
| (IBrI)-139 | −165.3 | −156.5 | 2.069 | 3.159 | 178.0 | 0.80 |
| (IBrI)-75 | −164.0 | −156.0 | 2.064 | 3.229 | 178.5 | 0.82 |

[a] The interaction energies of the optimized complexes were corrected for scaled (0.9887) zero point energy differences. [b] $R_i = XB_i/(rvdW_1 + rvdW_2)$ where $rvdW_1$ is the vdW radius of iodine (1.98 Å) and $rvdW_2$ is the Pauling ionic radius of bromide (1.95 Å).

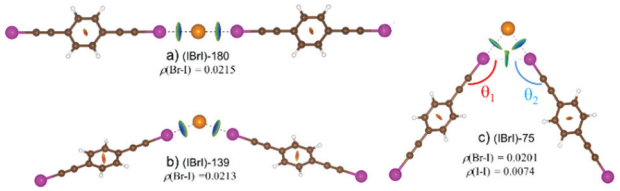


Fig. 7 Tridimensional NCI plots of (a) (IBrI)-180 in **1**; (b) (IBrI)-139 in **2**; and (c) (IBrI)-75 in **3**. The surfaces are colored in the [−0.03, 0.03] a.u. range of sign($\lambda_2$)$\rho$ (isosurface $s$ = 0.5).

Our understanding of non-covalent interactions in the trimers was completed by means of a non-covalent interaction (NCI) analysis. The tridimensional NCI plots corresponding to the three XB trimers considered are provided in Fig. 7. It is worth noting that in all the trimers, the I···Br$^-$ interaction has the typical profile of a halogen bond interaction, *i.e.*, it appears as a well-defined disk-shaped blue isosurface, which is indicative of a highly localized and attractive interaction. The electron density at the bond critical point was very similar in all cases, namely, 0.0227, 0.0237 and 0.0215 a.u. for (IBrI)-180, (IBrI)-139 and (IBrI)-75, respectively. Although this result is indicative of the similar strengths of the I···Br$^-$ interactions in the three trimers, it is noteworthy that the strength of the halogen bond interactions in (IBrI)-75 is slightly lower, as evidenced by its I···Br$^-$ distance being the longest and its electron density the lowest in the series. Interestingly, a lateral I···I contact was found in (IBrI)-75. This contact is characterized by a green isosurface between the two iodine atoms with a smooth shape and an electron density of 0.0079 a.u. at the bond critical point, which is characteristic of a dispersive interaction.[18] In order to attain a further understanding of the role of dispersive interactions in the trimers, we analyzed the dispersive contribution extracted from the D3BJ empirical dispersion correction scheme. Note that since all the trimers involve the same monomers, the difference in the dispersion term can be used to estimate the difference in the dispersive stabilization energy.[57] The dispersion contribution for the trimer (IBrI)-75 is about 8.0 kJ mol$^{-1}$ higher than that for the trimers (IBrI)-139 and (IBrI)-180. These results indicate that the dispersive stabilization energy in (IBrI)-75 is approximately 8.0 kJ mol$^{-1}$ more favorable than for the other trimers, in agreement with the NCI analysis, which shows an extra dispersive interaction between the iodine atoms in the trimer (IBrI)-75.

Halogen···halogen contacts between halogen atoms belonging to a molecule or a molecular fragment are usually classified into two categories based on their geometry, namely, type I ($\theta_1 \approx \theta_2$) (Fig. 7) and type II ($\theta_1 \approx 180^\circ$ and $\theta_2 \approx 90^\circ$). These contacts are chemically different in nature; type II contacts are actually standard halogen bonds, but type I contacts are considered to be van der Waals interactions.[58] As the NCI plot shows, (IBrI)-75 is supported by two halogen bonds with an I···Br$^-$ distance of 3.229 Å and by a symmetric non-halogen-bond *cis* type I I···I contact (optimized (IBrI)-75 data, $\theta_1$ = 126.1° and $\theta_2$ = 126.2°) with an I···I distance (optimized (IBrI)-75 data, 3.943 Å) close to the sum of the vdW radii of the two iodine atoms. Taken together, these contacts justify the interaction energy of (IBrI)-75 being similar to those of the other complexes, which have shorter I···Br$^-$ distances but lack this interaction (Table 4).

The relative energy variation among the trimers consisting of two p-BIB molecules bonded to a bromide anion as a function of the I···Br$^-$···I angle (energy is relative to the energy minimum, which appears at 90°) is represented in Fig. 8 (top). The halogen bond distance *vs.* the I···Br$^-$···I angle is shown in Fig. 8 (bottom). It is worth noting that as this angle increases from 75° to 180°, the relative energy initially decreases until the angle reaches 90° (energy minimum), after which the energy increases up to an angle of 180°. The energy difference between an angle of 75° and 90° is only 5.5 kJ mol$^{-1}$, and that between 90° and 180° is 7.6 kJ mol$^{-1}$.[14] The I···Br$^-$ length decreases

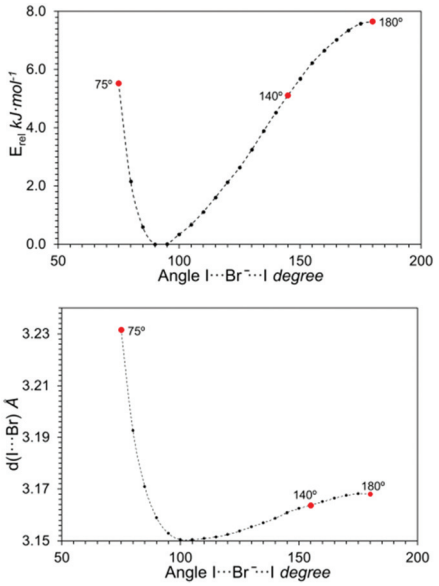


Fig. 8 Calculated energy differences between the trimer with minimum energy (90°) and the trimer with a given I···Br$^-$···I angle ($E_{rel}$) *vs.* the I···Br$^-$···I angle (top), and the calculated distances of the I···Br$^-$ halogen bond interaction ($d$(I···Br)) *vs.* the I···Br$^-$···I angle (bottom).

rapidly as the I···Br$^-$···I angle is increased from 75° to 90°, and then remains in the range between 3.15 and 3.17 Å from 90° to 180°. These results confirm that, as stated above, the I···Br$^-$ distance of (IBrI)-75 does not justify the energy of the interaction, and that when the I···Br$^-$···I angle is less than 90°, the I···Br$^-$ distance and the interaction energies of the trimers may be conditioned by a type I contact.

For each of the three crystal structures, different edge-to-edge *p*-BIB dimers were detected and studied to obtain a deeper understanding of the non-covalent interactions present in the crystals (Fig. 2). Single point calculations of p-BIB dimers extracted from experimental crystal structures were performed using DFT (see Experimental section). The interaction energies of all dimers (Table S6 in the ESI†) were computed using the 6-311G+(d,p) or 6-311G++(d,p) and DGDZVP (halogen atoms) basis sets. The 6-311G++(d,p) basis set was used to add an extra diffuse function to the hydrogen atoms, which may have important implications for the accuracy of hydrogen bond descriptions. However, the basis set did not have an observable effect on the interaction energies, and similar calculated interaction energies were obtained.[59] Furthermore, all of the calculated interaction energies were negative, *i.e.*, they were stabilizing.

The experimental I···H distances of complexes 2-a and 3-a were close to the sum of the vdW radii of iodine and hydrogen, but 1-a, 2-b and 3-b had slightly longer I···H distances (Fig. 2 and Table 3). The interaction energy of the HB dimer 1-a (−18.8 kJ mol$^{-1}$), which has two bifurcated hydrogen bonds, is clearly higher than those of the other HB dimers, although the I···H distances are longer than the sum of the vdW radii of the atoms involved. Additionally, **1** shows a *trans*-type I iodine···iodine contact ($\theta_1 = \theta_2 = 94.2°$, Fig. 9a) with an interaction energy of −5.0 kJ mol$^{-1}$.

In order to understand these dimers in more detail, an NCI analysis was applied; the tridimensional NCI plots are provided in Fig. 9. Non-conventional I···H hydrogen bonds[60] were revealed in all of the edge-to-edge *p*-BIB dimers, and appeared as defined disk-shaped surfaces. Moreover, π–π interactions between C–C triple bonds belonging to different monomers were identified and showed extended surface profiles characteristic of dispersive interactions.[61] The interaction energy of each dimer based on non-conventional hydrogen bonds was negative; this energy included all of the contacts that maintain the dimer, *i.e.*, the hydrogen bonds and the π–π interactions. It was revealed that the higher interaction energy of complex 1-a is probably due to its four hydrogen bonds, while the rest of the dimers only contain two.

The NCI analysis allowed us to further understand the nature of the interactions between *p*-BIB monomers. The existence of non-conventional hydrogen bonds was confirmed, in some cases, with contact distances slightly greater than the sum of the vdW radii. According to the experimental results, a type I iodine···iodine contact[58] was only detected in **1**, as shown by the green *s* isosurface between the two iodine atoms. The I···I distance of this interaction (*trans* type I contact) can be shorter or longer than the sum of the vdW radii of the atoms involved.[62] The experimental I···I distance was 4.572 Å, which is 15% longer than the sum of the vdW radii; however, the NCI analysis revealed this contact in the structure of **1**.

With the aim of analyzing these interactions in the crystal structures as a whole, an NCI analysis was also performed for the DFT optimized crystals. The tridimensional NCI plots for the three molecular co-crystals under study are provided in Fig. 10. For the sake of clarity, the cations have been omitted from Fig. 10, and their effect on the crystal structure will be analyzed later. Note that the same non-covalent interactions that were suggested for the trimers and dimers were observed in the crystal structures. Specifically, I···Br$^-$ halogen bonds were identified in the three crystals, and

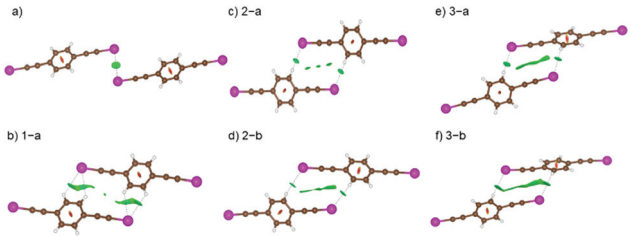


Fig. 9 Tridimensional NCI plots of (a) *trans* type I I···I in **1**, (b) 1-a, (c) 2-a, (d) 2-b, (e) 3-a, and (f) 3-b. Colored surfaces have sign($\lambda_2$)$\rho$ values of [−0.03, 0.03] a.u. (isosurface *s* = 0.5).

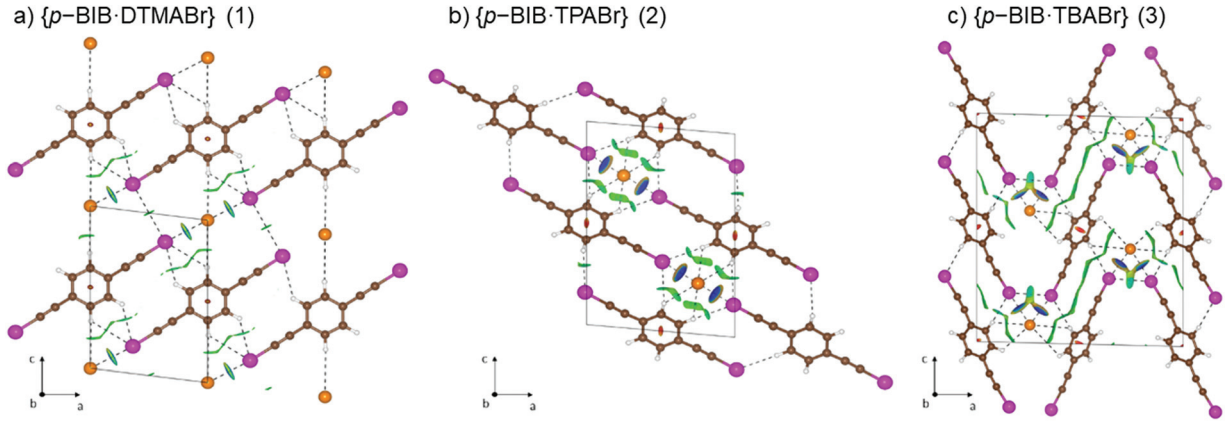


Fig. 10 Tridimensional NCI plots of (a) {p-BIB·DTMABr} (**1**), (b) {p-BIB·TPABr} (**2**), and (c) {p-BIB·TBABr} (**3**). Surfaces are colored in the [−0.03, 0.03] a.u. range of sign($\lambda_2$)$\rho$ (isosurface *s* = 0.5).

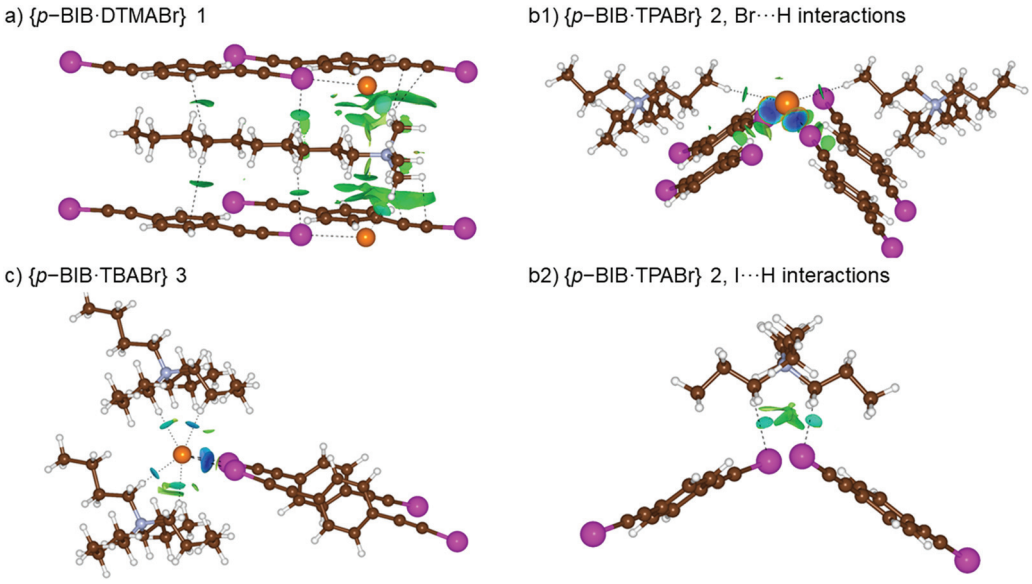


Fig. 11 Tridimensional NCI plots of the interaction between the base and the closest *p*-BIB molecules and bromide anions in (a) {*p*-BIB·DTMABr} (**1**), (b1) and (b2) {*p*-BIB·TPABr} (**2**), and (c) {*p*-BIB·TBABr} (**3**). Colored surfaces have sign($\lambda_2$)$\rho$ values of [−0.03, 0.03] a.u. (isosurface $s$ = 0.5). Note that, for the sake of clarity, the interactions involving **2** have been split into two views.

were characterized by well-defined disk-shaped blue isosurfaces. Moreover, non-conventional I···H hydrogen bonds were identified, as previously proposed for the dimer structures. Non-conventional $Br^-$···H hydrogen bonds were also identified, although these had not been detected in the crystal structure analysis. With respect to I···I contacts, the same interactions observed in the complexes were reproduced in the crystal structure. In particular, a type I I···I contact was revealed in **1** and **3** (Fig. 10a and c, respectively), in agreement with the Hirshfeld surface analysis.

Finally, we evaluated the key role of the cations in the crystal structure. The NCI plots of the interactions between a cation and the surrounding *p*-BIB molecules and bromide anions for the different crystals under study are presented in Fig. 11. The results show the dual effect of the cation. Firstly, a steric effect determines the crystal structure, as the *p*-BIB molecules and bromide anions adapt to the cation structure. This is the reason that **1** has a layered structure (DTMA is linear) and the *p*-BIB monomers in **2** and **3** exhibit angular arrangements (TPA and TBA are globular). Secondly, we also identified specific interactions between the cation and bromide or p-BIB. In particular, for **1** it was found that each DTMA cation establishes two $Br^-$··· ·H and two I···H non-conventional hydrogen bonds (which were also revealed by the sum of the vdW radii approach). These interactions exhibit well-defined disk-shaped isosurfaces, as depicted in Fig. 11a. Moreover, two H···benzene and H···triple C–C bond dispersive interactions were identified. For **2**, two I···H hydrogen bonds were observed (Fig. 11b1 and b2), and in both, the I··· ·H distance was lower than the sum of the vdW radii. In addition, the NCI analysis revealed two non-conventional $Br^-$···H hydrogen bonds, which had not been identified by either the vdW or ionic radii approach. Finally, in the case of **3**, four non-conventional $Br^-$···H hydrogen bonds were revealed, as depicted in Fig. 11c. Three of these bonds were identified by the sum of vdW and ionic radii approach.

## 4. Summary and conclusions

The halogen bonded co-crystals obtained from 1,4-bis-(iodoethynyl)benzene (*p*-BIB) with three bromide tetraalkylammonium salts (decyltrimethylammonium bromide, DTMABr; tetrapropylammonium bromide, TPABr; and tetrabutylammonium bromide, TBABr) are all heteromeric three-component systems. Tetraalkylammonium cations are weakly coordinating species that favor the formation of naked halide anions in solution. These naked anions act as very strong electron donors towards the electron-poor iodine atoms of *p*-BIB, which is a very good halogen bond donor molecule due to the sp hybridization of the carbon atoms linked to the iodine atoms. The crystal structures of the above-mentioned co-crystals suggest that the bromide anion has a preferential pattern of halogen bonding. In general, halides have a moderate bias towards the formation of two halogen bonds. This behavior is consistent with generalizations from the Cambridge Structural Database, which indicate that halide anions seem to have a bias towards the formation of two or three halogen bonds.

The analyses of the non-covalent interactions (NCIs) in both selected motifs, *i.e.*, dimers and trimers, and in the crystal structures show that the structures of **1** and **3** are stabilized by halogen bonds, type I halogen···halogen contacts, non-conventional hydrogen bonds, and π–π interactions. In fact, the NCI approach has confirmed the existence of additional non-covalent interactions not identified by a comparison of the interatomic distances with the sum of the tabulated vdW or ionic vdW radii.

The co-crystals detailed in this paper demonstrate that *p*-BIB represents a particularly robust and reliable tecton for XB-based coordination halides. Anion coordination and anion-templated assembly processes under XB control are still in their infancy, but they are expected to have a bright future. New

tectons in anion coordination chemistry will allow new families of supramolecular synthons to become involved in self-assembly and self-organization processes. NCI methodology has proved to be a valuable tool for understanding the role of supramolecular interactions in crystal structures.

## Conflicts of interest

There are no conflicts to declare.

## Acknowledgements

Thanks are given to the Crystallography Service of the University of Pais Vasco (Spain). J. M. acknowledges resources from the supercomputer ''memento'' and the technical assistance provided by BIFI-ZCAM. This work was supported by the Ministerio de Economía, Industria y Competitividad, under the projects PGC2018-093761-B-C31, PGC2018-097583-B-I00, and MAT2017-84838-P. The authors acknowledge support from Gobierno de Aragón-FEDER for funding the Crystal and Polymers Group (E47_20R, FEDER 2014–2020 Construyendo Europa desde Aragón).

## References

1 G. R. Desiraju, P. S. Ho, L. Kloo, A. C. Legon, R. Marquardt, P. Metrangolo, P. Politzer, G. Resnati and K. Rissanen, Definition of the halogen bond (IUPAC Recommendations 2013), *Pure Appl. Chem.*, 2013, **85**, 1711–1713.

2 C. B. Aakeröy, M. Baldrighi, J. Desper, P. Metrangolo and G. Resnati, Supramolecular Hierarchy among Halogen-Bond Donors, *Chem. – Eur. J.*, 2013, **19**, 16240–16247.

3 L. González, R. M. Tejedor, E. Royo, B. Gaspar, J. Munárriz, A. Chanthapally, J. L. Serrano, J. J. Vittal and S. Uriel, Two-Dimensional Arrangements of Bis(haloethynyl)benzenes Combining Halogen and Hydrogen Interactions, *Cryst. Growth Des.*, 2017, **17**, 6212–6223.

4 L. González, N. Gimeno, R. M. Tejedor, V. Polo, M. B. Ros, S. Uriel and J. L. Serrano, Halogen-bonding complexes based on bis(iodoethynyl)benzene units: A new versatile route to supramolecular materials, *Chem. Mater.*, 2013, **25**, 4503–4510.

5 P. Politzer, P. Lane, M. C. Concha, Y. Ma and J. S. Murray, An overview of halogen bonding, *J. Mol. Model.*, 2007, **13**, 305–311.

6 P. Politzer, J. S. Murray and T. Clark, Halogen bonding: An electrostatically-driven highly directional noncovalent interaction, *Phys. Chem. Chem. Phys.*, 2010, **12**, 7748–7757.

7 G. Cavallo, P. Metrangolo, T. Pilati, G. Resnati, M. Sansotera and G. Terraneo, Halogen bonding: a general route in anion recognition and coordination, *Chem. Soc. Rev.*, 2010, **39**, 3772–3783.

8 M. Fourmigué, and IUCr, Coordination chemistry of anions through halogen-bonding interactions, *Acta Crystallogr., Sect. B: Struct. Sci., Cryst. Eng. Mater.*, 2017, **73**, 138–139.

9 S. V. Lindeman, J. Hecht and J. K. Kochi, The charge-transfer motif in crystal engineering. Self-assembly of acentric (diamondoid) networks from halide salts and carbon tetrabromide as electron-donor/acceptor synthons, *J. Am. Chem. Soc.*, 2003, **125**, 11597–11606.

10 J. Lieffrig, A. G. Niassy, O. Jeannin and M. Fourmigué, Halogen-bonded halide networks from chiral neutral spacers, *CrystEngComm*, 2015, **17**, 50–57.

11 D. E. Barry, C. S. Hawes, S. Blasco and T. Gunnlaugsson, Structure Direction, Solvent Effects, and Anion Influences in Halogen-Bonded Adducts of 2,6-Bis(iodoethynyl)pyridine, *Cryst. Growth Des.*, 2016, **16**, 5194–5205.

12 R. Weiss, M. Rechinger, F. Hampel and A. Wolski, Stable 1: 1 Adducts from Iodoacetylenes and Iodide Ions: Ion Pair Strain as an Additional Driving Force?, *Angew. Chem., Int. Ed. Engl.*, 1995, **34**, 441–443.

13 J. Grebe, G. Geiseler, K. Harms and K. Dehnicke, Donor-acceptor complexes of halide ions with 1,4-diiodotetrafluorobenzene, *Z. Naturforsch., B: J. Chem. Sci.*, 1999, **54**, 77–86.

14 S. Triguero, R. Llusar, V. Polo and M. Fourmigue, Halogen bonding interactions of sym-triiodotrifluorobenzene with halide anions: A combined structural and theoretical study, *Cryst. Growth Des.*, 2008, **8**, 2241–2247.

15 N. L. Kilah, M. D. Wise and P. D. Beer, Crystallographic implications for the design of halogen bonding anion receptors, *Cryst. Growth Des.*, 2011, **11**, 4565–4571.

16 R. Laplaza, F. Peccati, R. A. Boto, C. Quan, A. Carbone, J. Piquemal, Y. Maday and J. Contreras-garcía, NCIPLOT and the analysis of noncovalent interactions using the reduced density gradient, *Wiley Interdiscip. Rev.: Comput. Mol. Sci.*, 2020, 1–18.

17 P. Bandyopadhyay and M. M. Seikh, Components of the interaction energy of the odd-electron halogen bond: an: ab initio study, *Phys. Chem. Chem. Phys.*, 2020, **22**, 15389–15400.

18 J. Munárriz, F. A. Rabuffetti and J. Contreras-García, Building Fluorinated Hybrid Crystals: Understanding the Role of Non-covalent Interactions, *Cryst. Growth Des.*, 2018, **18**, 6901–6910.

19 U. Siemens, *XSCANS. Siemens Analytical X-ray Instruments Inc.*, Madison, Wisconsin, 1994.

20 E. Oxford Diffraction, CrysAlis, Oxford Diffraction Ltd, Abingdon, Oxfordshire, CrysAlys, 2006.

21 G. M. Sheldrick, Crystal structure refinement with SHELXL, *Acta Crystallogr., Sect. C: Struct. Chem.*, 2015, **71**, 3–8.

22 S. K. Wolff, D. J. Grimwood, J. J. McKinnon, M. J. Turner, D. Jayatilaka and M. A. Spackman, CrystalExplorer (Version 3.1) University of Western Australia, CrystalExplorer (Version 3.1) Univ. West. Aust. 2012.

23 F. H. Allen and I. J. Bruno, Bond lengths in organic and metal-organic compounds revisited: X - H bond lengths from neutron diffraction data, *Acta Crystallogr., Sect. B: Struct. Sci.*, 2010, **66**, 380–386.

24 F. H. Allen, O. Kennard, D. G. Watson, L. Brammer, A. G. Orpen, R. Taylor and I. J. Bruno, Tables of Bond Lengths Determined by X-Ray and Neutron Diffraction. Part 1. Bond Lengths in Organic Compounds, *J. Chem. Soc., Perkin Trans. 2*, 1987, S1–S19.

25 M. J. Frisch, G. W. Trucks, H. B. Schlegel, G. E. Scuseria, M. A. Robb, J. R. Cheeseman, G. Scalmani, V. Barone, G. A. Petersson, H. Nakatsuji, X. Li, M. Caricato, A. Marenich, J. Bloino, B. G. Janesko, R. Gomperts, B. Mennucci, H. P. Hratchian, J. V. Ortiz, A. F. Izmaylov, J. L. Sonnenberg, D. Williams-Young, F. Ding, F. Lipparini, F. Egidi, J. Goings, B. Peng, A. Petrone, T. Henderson, D. Ranasinghe, V. G. Zakrzewski, J. Gao, N. Rega, G. Zheng, W. Liang, M. Hada, M. Ehara, K. Toyota, R. Fukuda, J. Hasegawa, M. Ishida, T. Nakajima, Y. Honda, O. Kitao, H. Nakai, T. Vreven, K. Throssell, J. J. A. Montgomery, J. E. Peralta, F. Ogliaro, M. Bearpark, J. J. Heyd, E. Brothers, K. N. Kudin, V. N. Staroverov, T. Keith, R. Kobayashi, J. Normand, K. Raghavachari, A. Rendell, J. C. Burant, S. S. Iyengar, J. Tomasi, M. Cossi, J. M. Millam, M. Klene, C. Adamo, R. Cammi, J. W. Ochtersk, R. L. Martin, K. Morokuma, O. Farkas, J. B. Foresman and D. J. Fox, *Gaussian 09, Revision A.02*, Gaussian Inc., Wallinford, CT, 2016.

26 C. T. Lee, W. T. Yang and R. G. Parr, Development of the colle-salvetti correlation-energy formula into a functional of the electron-density, *Phys. Rev. B: Condens. Matter Mater. Phys.*, 1988, **37**, 785–789.

27 A. D. Becke, Density-functional thermochemistry. 3. The role of exact exchange, *J. Chem. Phys.*, 1993, **98**, 5648–5652.

28 A. D. Becke, A new mixing of Hartree-Fock and local density-functional theories, *J. Chem. Phys.*, 1993, **98**, 1372–1377.

29 H. Grimme, S. Antony, J. Ehrlich, S. Krieg, S. Grimme, J. Antony, S. Ehrlich and H. Krieg, A consistent and accurate ab initio parametrization of density functional dispersion correction (DFT-D) for the 94 elements H-Pu, *J. Chem. Phys.*, 2010, **132**, 154102.

30 S. Grimme, S. Ehrlich and L. Goerigk, Effect of the damping function in dispersion corrected density functional theory, *J. Comput. Chem.*, 2011, **32**, 1450–1495.

31 R. Krishnan, J. S. Binkley, R. Seeger and J. A. Pople, Self-consistent molecular orbital methods. XX. A basis set for correlated wave functions, *J. Chem. Phys.*, 1980, **72**, 650–654.

32 N. Godbout, D. R. Salahub, J. Andzelm and E. Wimmer, Optimization of Gaussian-type basis sets for local spin density functional calculations. Part I. Boron through neon, optimization technique and validation, *Can. J. Chem.*, 1992, **70**, 560–571.

33 H. Bernhard Schlegel, Optimization of equilibrium geometries and transition structures, *J. Comput. Chem.*, 1982, **3**, 214–218.

34 F. Weigend and R. Ahlrichs, Balanced basis sets of split valence, triple zeta valence and quadruple zeta valence quality for H to Rn: Design and assessment of accuracy, *Phys. Chem. Chem. Phys.*, 2005, **7**, 3297–3305.

35 K. A. Peterson, D. Figgen, E. Goll, H. Stoll and M. Dolg, Systematically convergent basis sets with relativistic pseudopotentials. II. Small-core pseudopotentials and correlation consistent basis sets for the post-d group 16–18 elements, *J. Chem. Phys.*, 2003, **119**, 11113–11123.

36 S. F. Boys and F. Bernardi, Calculation of small molecular interaction by differences of separate total energies -Some procedures with reduced errors, *Mol. Phys.*, 1970, **19**, 553–566.

37 J. P. Merrick, D. Moran and L. Radom, An Evaluation of Harmonic Vibrational Frequency Scale Factors, *J. Phys. Chem. A*, 2007, **111**, 11683–11700.

38 J. George, C. Reimann, V. L. Deringer, T. Bredow and R. Dronskowski, On the DFT ground state of crystalline bromine and iodine, *ChemPhysChem*, 2015, **16**, 728–732.

39 E. R. Johnson, S. Keinan, P. Mori-Sá Nchez, J. Contreras-García, A. J. Cohen and W. Yang, Revealing Noncovalent Interactions, *J. Am. Chem. Soc.*, 2010, **132**, 6498–6506.

40 J. Contreras-García, E. R. Johnson, S. Keinan, R. Chaudret, J. P. Piquemal, D. N. Beratan, W. Yang, P. Piquemal, D. N. Beratan, W. Yang, J. P. Piquemal, D. N. Beratan and W. Yang, NCIPLOT: A program for plotting noncovalent interaction regions, *J. Chem. Theory Comput.*, 2011, **7**, 625–632.

41 A. Otero-de-la-Roza, E. R. Johnson and V. Luaña, Critic2: A program for real-space analysis of quantum chemical interactions in solids, *Comput. Phys. Commun.*, 2014, **185**, 1007–1018.

42 K. Momma and F. Izumi, VESTA 3 for three-dimensional visualization of crystal, volumetric and morphology data, *J. Appl. Crystallogr.*, 2011, **44**, 1272–1276.

43 W. Wu and H. Jiang, Haloalkynes: A Powerful and Versatile Building Block in Organic Synthesis, *Acc. Chem. Res.*, 2014, **47**, 2483–2504.

44 F. Kniep, L. Rout, S. M. Walter, H. K. V. Bensch, S. H. Jungbauer, E. Herdtweck and S. M. Huber, 5-Iodo-1,2,3-triazolium-based multidentate halogen-bond donors as activating reagents, *Chem. Commun.*, 2012, **48**, 9299–9301.

45 T. Nishikawa, S. Shibuya and S. Hosokawa, One Pot Synthesis of Haloacetylenes from Trimethylsilylacetylenesynlett, *Synlett*, 1994, 485–486.

46 K. Bouchmella, B. Boury, S. G. Dutremez and A. Van Der Lee, Molecular assemblies from imidazolyl-containing haloalkenes and haloalkynes: Competition between halogen and hydrogen bonding, *Chem. – Eur. J.*, 2007, **13**, 6130–6138.

47 A. Velazquez-Campoy and E. Freire, Isothermal titration calorimetry to determine association constants for high-affinity ligands, *Nat. Protoc.*, 2006, **1**, 186–191.

48 A. Velazquez-Campoy, S. A. Leavitt and E. Freire, *Protein-Protein Interactions: Methods and Applications: Second Edition*, Springer, New York, 2015, pp. 183–204.

49 S. M. Walter, F. Kniep, L. Rout, F. P. Schmidtchen, E. Herdtweck and S. M. Huber, Isothermal calorimetric titrations on charge-assisted halogen bonds: Role of entropy, counterions, solvent, and temperature, *J. Am. Chem. Soc.*, 2012, **134**, 8507–8512.

50 S. Chakraborty, R. Dutta and P. Ghosh, Halogen bonding assisted selective removal of bromide, *Chem. Commun.*, 2015, **51**, 14793–14796.

51 R. Tepper, B. Schulze, M. Jäger, C. Friebe, D. H. Scharf, H. Görls and U. S. Schubert, Anion Receptors Based on Halogen Bonding with Halo-1,2,3- triazoliums, *J. Org. Chem.*, 2015, **80**, 3139–3150.

52 S. H. Jungbauer, S. Schindler, E. Herdtweck, S. Keller and S. M. Huber, Multiple Multidentate Halogen Bonding in Solution, in the Solid State, and in the (Calculated) Gas Phase, *Chem. – Eur. J.*, 2015, **21**, 13625–13636.
53 G. R. Desiraju and R. Parthasarathy, The Nature of Halogen-···Halogen Interactions: Are Short Halogen Contacts Due to Specific Attractive Forces or Due to Close Packing of Non-spherical Atoms?, *J. Am. Chem. Soc.*, 1989, **111**, 8725–8726.
54 H. M. Yamamoto, R. Maeda, J.-I. Yamaura and R. Kato, Structural and physical properties of conducting cation radical salts containing supramolecular assemblies based on p-bis(iodoethynyl)benzene derivatives, *J. Mater. Chem.*, 2001, **11**, 1034–1041.
55 P. A. Wood, J. J. McKinnon, S. Parsons, E. Pidcock and M. A. Spackman, Analysis of the compression of molecular crystal structures using Hirshfeld surfaces, *CrystEngComm*, 2008, **10**, 368–376.
56 M. A. Spackman and D. Jayatilaka, Hirshfeld surface analysis, *CrystEngComm*, 2009, **11**, 19–32.
57 M. Bursch, E. Caldeweyher, A. Hansen, H. Neugebauer, S. Ehlert and S. Grimme, Understanding and Quantifying London Dispersion Effects in Organometallic Complexes, *Acc. Chem. Res.*, 2019, **52**, 258–266.
58 A. Mukherjee and G. R. Desiraju, Halogen bonds in some dihalogenated phenols: Applications to crystal engineering, *IUCrJ*, 2014, **1**, 49–60.
59 E. Papajak, J. Zheng, X. Xu, H. R. Leverentz and D. G. Truhlar, Perspectives on Basis Sets Beautiful: Seasonal Plantings of Diffuse Basis Functions, *J. Chem. Theory Comput.*, 2011, **7**, 3027–3034.
60 I. Alkorta, I. Rozas and J. Elguero, Non-conventional hydrogen bonds, *Chem. Soc. Rev.*, 1998, **27**, 163.
61 M. Alonso, T. Woller, F. J. Martín-Martínez, J. Contreras-García, P. Geerlings and F. De, Proft, Understanding the fundamental role of dispersion interactions in shaping carbon-based materials, *Chem. – Eur. J.*, 2014, **20**, 4931–4941.
62 B. Li, M. Dong, H. Fan, C. Feng and S. Zang, Halogen-···Halogen Interactions in the Assembly of High-Dimensional Supramolecular Coordination Polymers Based on 3,5-Diiodobenzoic Acid, *Cryst. Growth Des.*, 2014, **14**, 6325–6336.